

# ATLAS TileCal Submodule B-field Measurement

J.A.Budagov, S.B.Fedorenko, V.V.Kalinichenko, Yu.Ph.Lomakin, S.B.Vorojtsov  
*Joint Institute for Nuclear Research, Dubna, Russia*  
M.Nessi  
*CERN, Geneva, Switzerland*

## Contents

<b>1</b>	<b>Introduction</b>	<b>2</b>
<b>2</b>	<b>Experimental Setup</b>	<b>2</b>
2.1	Preparation for the measurements . . . . .	2
2.2	Measurement device . . . . .	2
2.2.1	Magnetometer . . . . .	2
2.2.2	DC Stabilizer . . . . .	3
2.2.3	Hall Probe . . . . .	4
<b>3</b>	<b>Results</b>	<b>5</b>
3.1	Data structure . . . . .	5
3.2	Data Analysis . . . . .	8
<b>4</b>	<b>Conclusion</b>	<b>8</b>

# 1 Introduction

This work pursues the following goals:

- To cross check of the previous measurement done at CERN [1], [2].
- To simulate of the magnetic structure in the vicinity of the symmetry plane of the TileCal where the probability of the magnetic flux penetration to tiles is the highest due to symmetry condition [3], [4].

## 2 Experimental Setup

### 2.1 Preparation for the measurements

To perform magnetic measurements for submodule the magnet E2 with the pole diameter 1.36 m and maximal air gap  $\approx 300$  mm was chosen. This magnet had been used for some other experiment with the field level  $\approx 2.2$  T and air gap  $\approx 30$  mm. So, to prepare the magnet for our measurement, the pole shoes were dismantled to get the required air gap  $\approx 300$  mm and it demagnetized.

Submodule field measurement was done for three its position in respect to the pole tip (see Figure 1). For every submodule position the magnet was demagnetized prior to the field measurement.

In Figure 1 the submodule 3 situates in between the magnet pole tips 1 and 2 with the  $\approx 3$  mm nonmagnetic spacer 4 being inserted between the submodule and the lower pole 2 and  $\approx 3$  mm air gap 5 between the submodule and the upper magnet pole 1.

Magnet demagnetization was performed setting to maximal value of the excitation coil current from the previous experiment. After  $\approx 3$  min the current was reversed with decreasing the current value by  $\approx 3\%$ . This step was repeated until the excitation current became approximately zero.

### 2.2 Measurement device

#### 2.2.1 Magnetometer

Figure 2 is a simplified block diagram of the magnetometer used in the magnetic test of the submodule. Functionally, the components may be placed in two main groups: Hall current supply and Hall voltage measurement.

The Hall current supply consists of a direct current stabilizer (DCS) and its direct current power supplies (DCPS). The DC stabilizer provides a stable current of  $\approx 90$  mA to the control side of the Hall probe.

The second system includes a Hall probe (HP) itself and a digital voltmeter (DV). The function of this system is to show an operator the voltage which is proportional to the magnetic field being measured. The integrating digital voltmeter is a model V7-34A.

Model V7-34A specifications:

- **Ranges** 100 mV and 1,10,100 and 1000 V full scale selected by front panel switch, external programming or autoranger.

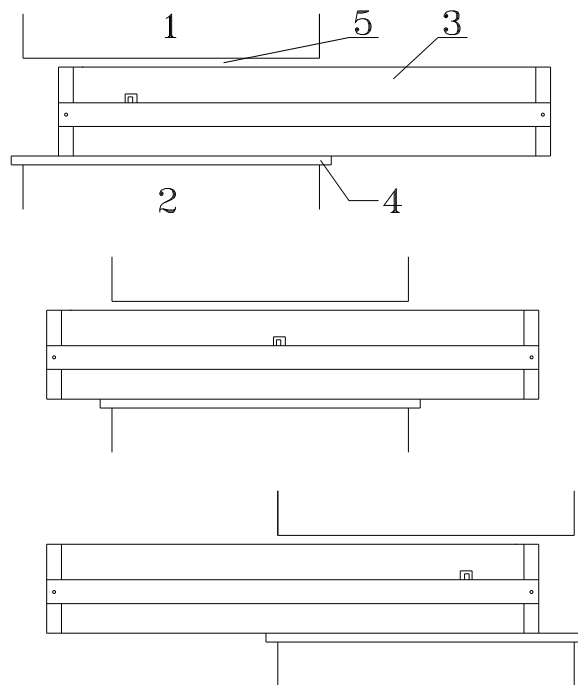


Figure 1:

- **Input impedance:** greater than 2000 MW on 100 mV; 10 MW on 100 and 1000 V; 20000 MW on 1 and 10 V.
- **Accuracy:**
  - $\pm 0.02\%$  rdg  $\pm 0.01\%$  fc on 100 mV;
  - $\pm 0.015\%$  rdg  $\pm 0.002\%$  fc on 1, 100, 1000 V;
  - $\pm 0.01\%$   $\pm 0.002\%$  rdg  $\pm 0.002\%$  fc on 10 V.
- **Resolution:** 100 mV range displays readings to 1 mV.

### 2.2.2 DC Stabilizer

Figure 3 is a schematic diagram of the DC stabilizer [5] which supplies a  $\approx 90$  mA direct current to the input of the Hall probe. This stabilizer is of compensation type and consists of a reference voltage source, a voltage comparator (a differential amplifier DA2), a current amplifier (a transistor VT1) and a reference resistor.

The reference voltage source [6] consists of an operational amplifier DA1, a Zener diode VD1 and four very stable resistors R1-R4. The reference resistor includes four very stable resistors R5,R6,R7 and R9. Running through the reference resistor, the output current is converted into voltage, which is applied to one input of DA2. The reference voltage is applied to the other input of DA2. The output of DA2 is fed to the current amplifier VT1.

### 2.2.3 Hall Probe

The indium antimonide Hall probe used in this measurement is a model PKhE 606. This device is characterized by low input and output impedance, high sensitivity, good linearity, and low temperature dependence. Figure 4 shows the dimensions of the unit.

The open circuit sensitivity of the unit is 0.76 V/AT, while the input and output impedances are 3.88 and 4.45 ohms, respectively. The temperature coefficient for the Hall constant is 0.002 %/K. There is a null voltage (i.e. a signal output for no magnetic field) which is caused by certain unavoidable inaccuracies in the construction of the unit. This is  $6 \times 10^{-6}$  V for a control current of 100 mA.

Breakage is a major problem in working with the fragile Hall probe. For this reason it was decided to package the Hall probe with its cable in an epoxy module together with a mount. Figure 5 shows this module. The mount length is 1.77 meters. The design of the mount was dictated by the size and geometry of the submodule tested and the test electromagnet.

Experimental set up provides a true measurement accuracy of order  $\pm 1\%$ .

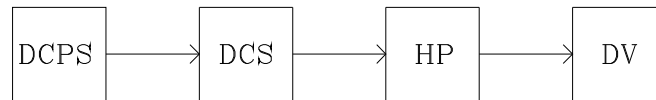


Figure 2:

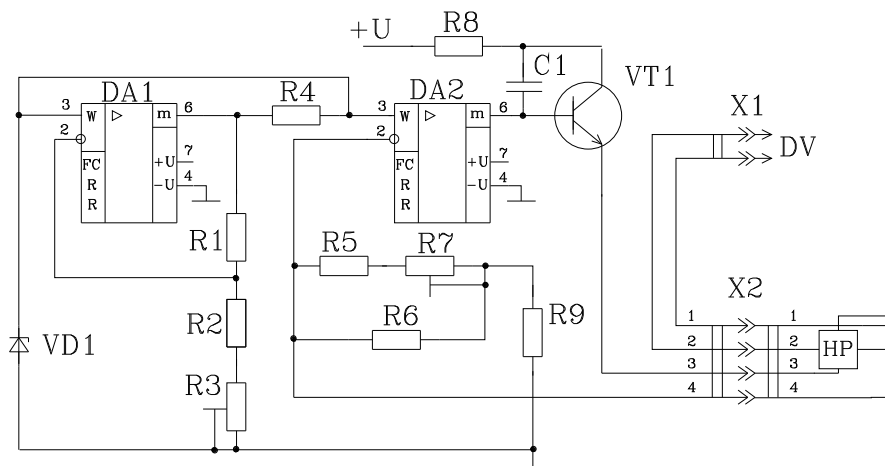


Figure 3:

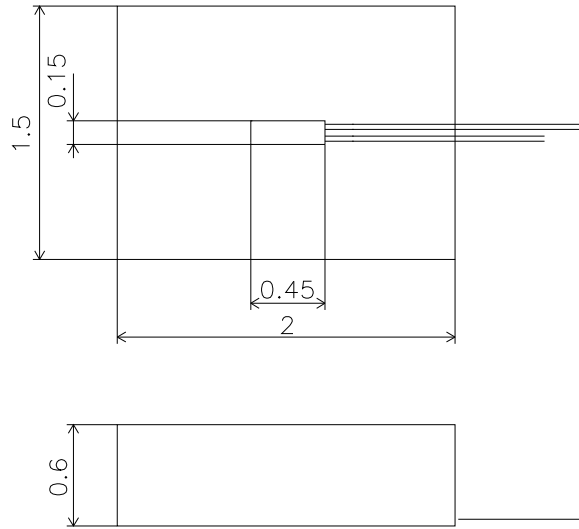


Figure 4:

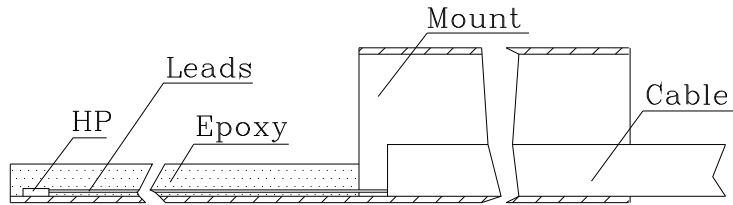


Figure 5:

## 3 Results

### 3.1 Data structure

The schematic view of the submodule tile structure is given in Figure 6. There one can see the magnet air gap midplane position in respect to the tile structure. Tile layers are directed in parallel to the midplane and the tile rows are placed normal to the midplane. There are 11 tile rows. Tile slots are arranged in a staggered order. The external magnetic field direction is normal to the wider part of the tile and (naturally) normal to the midplane.

External magnetic field measurement were conducted at the outer surface of the submodule. The internal field in the tile slots was measured for the tile layer at the midplane and for the layers above and below the midplane. The field value along row 4 was also measured.

The shielding capability of the submodule (shielding coefficient  $K_{shield}$ ) was defined as a ratio of the external field level to the field within the tile slot under consideration. Two levels of the external field were applied: 108 Gs and 400 Gs. The results were compared with the similar measurements, performed at CERN (see [1])

The results of the measurements are given below in Table 1—Table 4 and also displayed

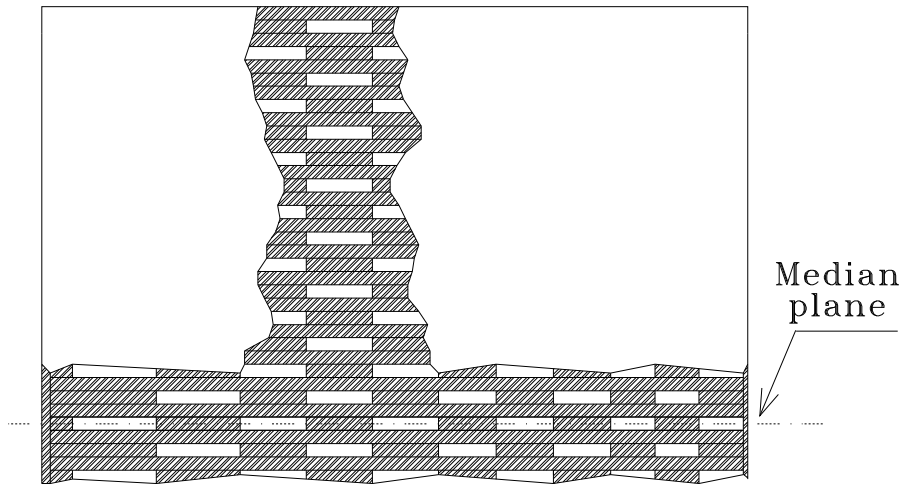


Figure 6:

in Figures 7— 10. The following notation is used there:

- **n** — number of row, starting from the narrow part of the submodule in the direction of its wider side (girder).
- **b-e-1** — external field at the outer submodule surface (field level of  $\approx 108Gs$ )
- **b-I-1** — internal field at the tile locations for the external field level of  $\approx 108Gs$ 
  - **m** means the midplane layer,
  - **u** means the layer above the midplane,
  - **d** means the layer below the midplane,
- **k-1**—K-shielding for the external field level of  $\approx 108Gs$
- **b-e-4**— external field at the outer submodule surface (field level of  $\approx 400Gs$ )
- **b-I-4**— internal field at the tile locations for the external field level of  $\approx 400Gs$
- **k-4**— K-shielding for the external field level of  $\approx 400Gs$
- **I** number of layers for the slots in row 4 (from the upper surface until the lower surface of the submodule). There is no slot in the midplane for this row.
- **kn4**— K-shielding for the 4<sup>th</sup> tile row, depending on the number of layer “I” (the field level of  $\approx 400Gs$ )
- **kfb**— shielding coefficient from Ref.[1] for the external field level of  $\approx 105Gs$

**Table 1**

n	b-e-1	b-I-1m	k-1m	b-e-4	b-I-4m	k-4m
1	152	39.1	2.76	614	114.1	3.50
3	138	39.0	2.76	568	109.8	3.64
5	116	34.2	3.15	501	95.2	4.20
7	112	40.7	2.65	467	120.3	3.32
9	108	36.0	3.00	445	105.9	3.77
11	126	27.8	3.88	436	85.6	4.67

**Table 2**

n	b-e-1	b-i-1u	k-1u	b-i-1d	k-1d	b-e-4	b-i-4u	k-4u	b-i-4d	k-4d
2	132	34.2	3.15	41.8	2.62	563	107.4	3.72	129.1	3.09
4	108	38.1	2.83	40.0	2.70	489	107.2	3.73	112.2	3.56
6	94	35.7	3.02	47.0	2.29	431	97.9	4.08	136.8	2.92
8	95	34.2	3.15	45.2	2.38	407	96.2	4.15	135.7	2.94
10	95	28.3	3.81	33.9	3.18	388	92.3	4.33	100.8	3.97

**Table 3**

l	1	2	3	4	5	6	7	8
kn4	2.90	3.50	3.54	3.86	3.49	3.65	4.42	4.23
l	9	10	11	12	13	14	15	16
kn4	3.08	3.80	3.50	3.67	3.27	3.75	3.83	3.08

**Table 4**

n	1	2	3	4	5	6	7	8	9	10	11
kfb-u	2.39	3.00	2.84	2.50	2.44	2.50	2.44	2.28	2.33	1.98	2.84
kfb-d	3.18	3.62	3.00	2.39	2.14	2.14	1.94	2.06	2.39	2.19	2.84

## 3.2 Data Analysis

- In Figure 7 one can see that the average shielding factor, measured in Ref. [1], is  $\approx 2.4$ . In our measurements for the same external field level it is  $\approx 2.9$ , which is  $\approx 20\%$  higher. As the external field level increases up to 400–600 Gs, the  $K_{shield}$  is getting as high as  $\approx 3.5$ . This leads to even greater suppression of the tile location field ( $B_{tiles}$ ), i.e. the tile field grows not proportional of the external field level by much less than that. This effect can be explained by the iron core permeability increasing when the field level is less than 8 kGs [7].
- According to the results of the measurement, presented in Figure 8 and Figure 9,  $B_{tiles} \leq 150$  Gs when the external field level  $\leq 500$  Gs.
- In the above mentioned Figures one can see that the external field distribution decreases from the narrow part of the submodule to the girder side. This can be explained by the higher magnetization of the narrow part of the submodule.
- There is also waving behavior of the external field curves which reflect the tile structure of the submodule with its different magnetic conductivity in the tile slots and in the iron spacers between them. The effect has been already noticed in the calculations (See Ref. [2]).
- In Figures 8– 10 one can notice lack of the symmetry in the field values, which one could expect due to the local symmetry in the tile structure. The reason for this effect could be the tile slot height deviation from the required value 4 mm. In Figure 10 the results of the slot height measurements for the inlet ( $hi$ ) and exit ( $he$ ) of the slots are presented. This effect of course will change  $K_{shield}$  and the magnetic flux redistribution between the individual slots and iron spacers. One can also see the strong correlation between  $K_{shield}$  and the slot height in the Figure.
- In Figure 10 the edge effect is also noticeable:  $K_{shield}$  decreases for the 1<sup>st</sup> and 16<sup>th</sup> tile layers. This effect has been also noticed in the calculations (See Ref. [2]).

## 4 Conclusion

- The result of this measurement in general confirms the data given in Ref. [1], but the shielding capability of the submodule under consideration was  $\approx 20\%$  higher than in Ref. [1].
- $B_{tiles} \leq 150$  Gs up to the external field level 500 Gs and the tile field grows much less than the external field level in this range.
- The data obtained in this measurement could be used as a benchmark when producing a computer model of the TileCal magnetic field distribution.

Authors would like to acknowledge the help of Drs. Ivashkevich S.A. and Mrs. Kazakova G.G. in conducting the measurements.



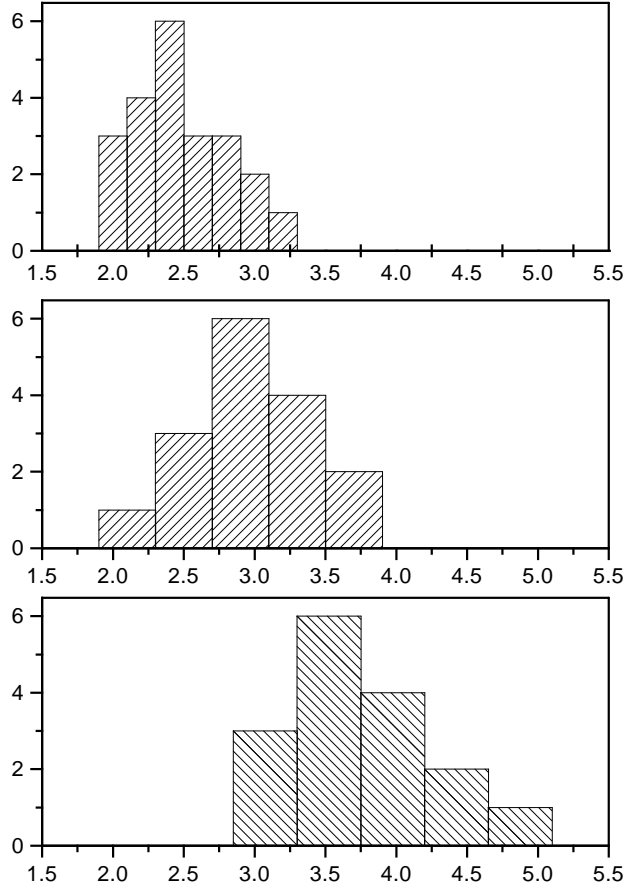


Figure 7:  $K_{shielding}$  for the midplane, upper and lower layers

## References

- [1] F.Bergsma. Magnetic Field Model for ATLAS, Improvements on Tile-calorimeter Model. Transparencies shown at the Toroid Meeting (Magnetic Field) held at CERN 12.07.95.
- [2] S.B.Vorozhtsov, I.V.Titkova, M.Nessi. TILE-No-58. "Contribution to the ATLAS B-field 3D Model". 11-SEP-95. Communication of the JINR. E-9-96-168, JINR, Dubna, 1996.
- [3] M.Nessi, J.A.Budagov, S.B.Vorozhtsov, O.N.Borisov, O.V.Lomakina, G.A.Karamysheva. "Computer Models for the TILECAL Magnetic Field". Communication of the JINR. B-1-95-162, JINR, Dubna, 1995.
- [4] M.Nessi, F.Bergsma, S.B.Vorozhtsov, O.N.Borisov, O.V.Lomakina. "TileCal Magnetic Field Simulation". Communication of the JINR. B-1-95-163, JINR, Dubna, 1995

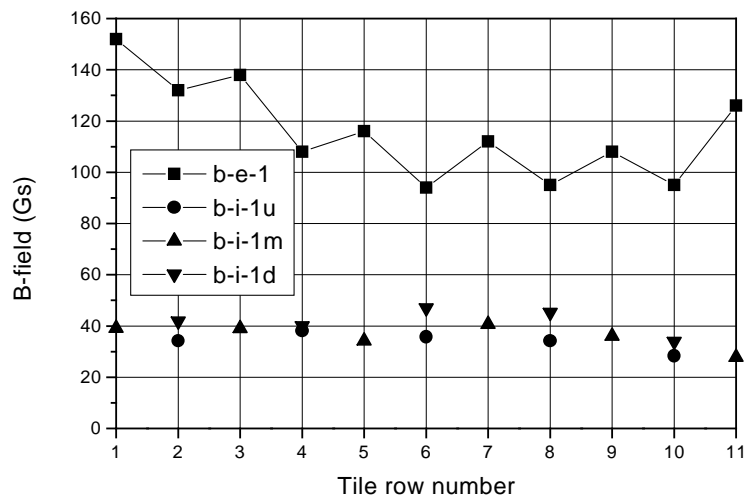


Figure 8: External and tile location fields at the field level of 108 Gs

- [5] Ivashkevich S.A., Kazakova G.G. Hall-Effect Device of High Accuracy. JINR Communication P13-91-283, Dubna, 1991.
- [6] Horowitz P., Hill W. The Art of Electronics. Moscow, Mir, 1993
- [7] V.V.Kalinichenko, S.B.Fedorenko. "Magnetic Property Measurements of Steel for TileCal". ATLAS Internal Note. TILECAL-No-059. September 11, 1995.

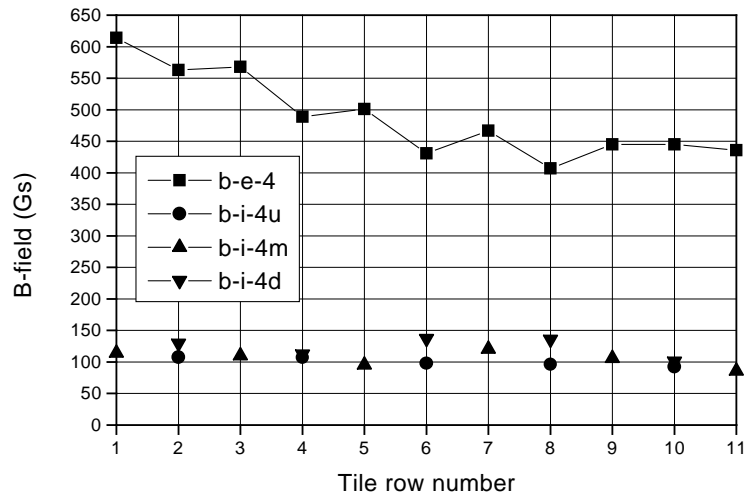


Figure 9: External and tile location fields at the field level of 400 Gs

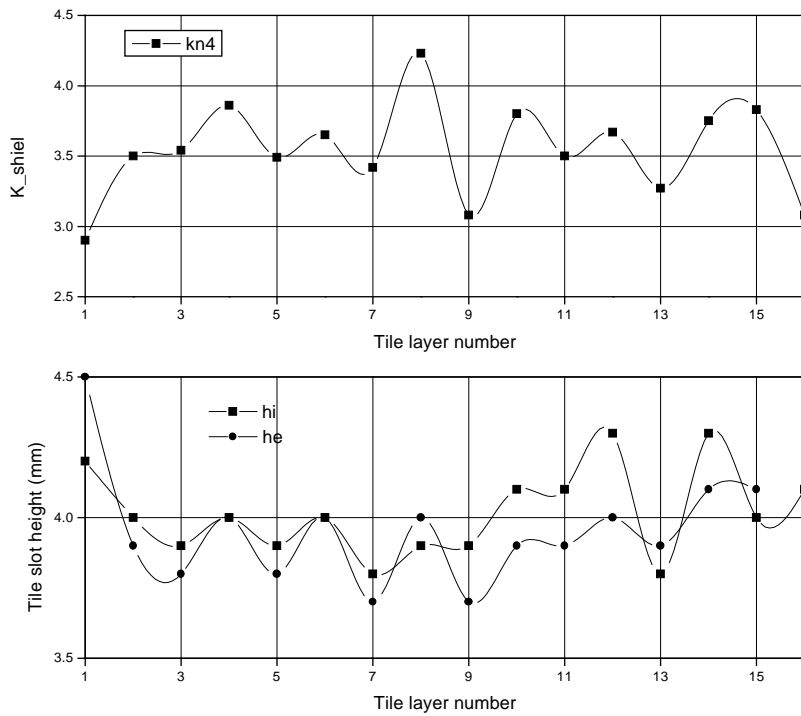


Figure 10: Tile location field in the 4th row at the external field level of 400 Gs (upper plot) and tile slot height measurements